Title

Human CYP2A13 and CYP2F1 Mediate Naphthalene Toxicity in the Lung and Nasal Mucosa of CYP2A13/2F1-Humanized Mice

Journal

Environmental Health Perspectives, 125(6)

ISSN

1542-4359

Authors

Li, Lei
Carratt, Sarah
Hartog, Matthew
et al.

Publication Date

2017-06-23

DOI

10.1289/ehp844

Peer reviewed

A Section 508–conformant HTML version of this article is available at https://doi.org/10.1289/EHP844.

Human CYP2A13 and CYP2F1 Mediate Naphthalene Toxicity in the Lung and Nasal Mucosa of CYP2A13/2F1-Humanized Mice

Lei Li,[1] Sarah Carratt,[2] Matthew Hartog,[3] Nataliia Kovalchuk,[1] Kunzhi Jia,[1] Yanan Wang,[1] Qing-Yu Zhang,[1] Patricia Edwards,[2] Laura Van Winkle,[2] and Xinxin Ding[3]

[1]Wadsworth Center, New York State Department of Health, Albany, New York, USA
[2]Center for Health and the Environment, University of California, Davis (UC Davis), Davis, California, USA
[3]College of Nanoscale Science and Engineering, State University of New York (SUNY) Polytechnic Institute, Albany, New York, USA

Background: The potential carcinogenicity of naphthalene (NA), a ubiquitous environmental pollutant, in human respiratory tract is a subject of intense debate. Chief among the uncertainties in risk assessment for NA is whether human lung CYP2A13 and CYP2F1 can mediate NA's respiratory tract toxicity.

Objectives: We aimed to assess the *in vivo* function of CYP2A13 and CYP2F1 in NA bioactivation and NA-induced respiratory tract toxicity in mouse models.

Methods: Rates of microsomal NA bioactivation and the effects of an anti-CYP2A antibody were determined for lung and nasal olfactory mucosa (OM) from *Cyp2abfgs*-null, CYP2A13-humanized, and CYP2A13/2F1-humanized mice. The extent of NA respiratory toxicity was compared among wild-type, *Cyp2abfgs*-null, and CYP2A13/2F1-humanized mice following inhalation exposure at an occupationally relevant dose (10 ppm for 4 hr).

Results: *In vitro* studies indicated that the NA bioactivation activities in OM and lung of the CYP2A13/2F1-humanized mice were primarily contributed by, respectively, CYP2A13 and CYP2F1. CYP2A13/2F1-humanized mice showed greater sensitivity to NA than *Cyp2abfgs*-null mice, with greater depletion of nonprotein sulfhydryl and occurrence of cytotoxicity (observable by routine histology) in the OM, at 2 or 20 hr after termination of NA exposure, in humanized mice. Focal, rather than gross, lung toxicity was observed in *Cyp2abfgs*-null and CYP2A13/2F1-humanized mice; however, the extent of NA-induced lung injury (shown as volume fraction of damaged cells) was significantly greater in the terminal bronchioles of CYP2A13/2F1-humanized mice than in *Cyp2abfgs*-null mice.

Conclusion: CYP2F1 is an active enzyme. Both CYP2A13 and CYP2F1 are active toward NA in the CYP2A13/2F1-humanized mice, where they play significant roles in NA-induced respiratory tract toxicity. https://doi.org/10.1289/EHP844

Introduction

Naphthalene (NA), commonly found in diesel exhaust, biomass burning, and tobacco smoke (Kakareka and Kukharchyk 2003; U.S. EPA 1986; Witschi et al. 1997), is an important environmental pollutant. The respiratory tract toxicity of NA has been studied extensively in rodents. The results of the National Toxicology Program chronic rodent bioassays for NA found significant, dose-dependent increases in alveolar adenomas in the lungs of female mice and in adenomas and neuroblastomas of the nasal epithelium in rats (Abdo et al. 1992; Abdo et al. 2001). However, the potential carcinogenicity of NA in human respiratory tract is a subject of intense debate. The mechanism of NA carcinogenicity is thought to involve repeated cycles of injury and repair related to acute cytotoxicity following bioactivation of NA by cytochrome P450 (P450) enzymes, because there is an extremely strong correlation between the sites of tumor formation in rodent models and the sites of acute cytotoxicity in the lung (Brusick 2008; Buckpitt et al. 2002). Thus, P450-mediated bioactivation of NA and the consequent acute cytotoxicity is the key step to initiate NA carcinogenicity. Previous studies in mice have demonstrated the essential roles of mouse CYP2F2 in pulmonary toxicity of NA (Li et al. 2011) and mouse CYP2A5 in nasal toxicity of NA (Hu et al. 2014); these studies also illustrated the tissue-specific nature of the contributions of individual P450 enzymes to NA toxicity. Nevertheless, chief among the uncertainties in human risk assessment for NA is whether human lung CYP2A13 and CYP2F1 can mediate the respiratory tract toxicities of NA.

Human CYP2A13 and CYP2F1 are preferentially expressed in the respiratory tract, with little or no expression in other tissues (Carr et al. 2003; Su et al. 2000; Weems and Yost 2010; Zhang and Ding 2008). CYP2A13, a highly efficient enzyme for the bioactivation of several known lung carcinogens, including several nitrosamine compounds (Su et al. 2000), has been reported to bioactivate NA to toxic naphthoquinone metabolites *in vitro* (Fukami et al. 2008), but NA metabolism by CYP2F1 has not been fully characterized, due in large part to the difficulties in producing functional CYP2F1 in heterologous expression systems (Baldwin et al. 2005; Behrendorff et al. 2012; Lanza et al. 1999; Wei et al. 2012). The expression of recombinant CYP2F1 in mammalian cells yielded very low levels of expression; however, studies using CYP2F1 from this source suggested that it was active toward a number of compounds, particularly 3-methylindole (Lanza et al. 1999), but it had very low activity toward NA (Lanza et al. 1999), relative to rates reported for mouse CYP2F2 (Shultz et al. 1999) or rat CYP2F4 (Baldwin et al. 2005). Such a species difference between rodent and human CYP2F enzymes in the activity toward NA bioactivation would argue against possible carcinogenicity of NA in human respiratory tract. Therefore, a better assessment of the ability of human CYP2F1, as well as CYP2A13, to bioactivate NA, both *in vitro* and *in vivo*, is important for assessing human health risks from exposure to this ubiquitous pollutant.

We recently reported the generation and initial characterization of a CYP2A13/2B6/2F1-transgenic (TG) mouse model, which exhibited a human-like tissue-selective co-expression of CYP2A13 and CYP2F1 in the respiratory tract, but liver-specific

Address correspondence to L. Van Winkle, Center for Health and the Environment, Building 3792, Room 129, Old Davis Rd., UC Davis, Davis, CA 95616 USA. Telephone: (530) 754-9060. E-mail: lsvanwinkle@ucdavis.edu, and X. Ding, College of Nanoscale Science and Engineering, SUNY Polytechnic Institute, 257 Fuller Rd., NanoFab East, Albany, NY 12203 USA. Telephone: (518) 956-7057. E-mail: xding@sunypoly.edu

Supplemental Material is available online (https://doi.org/10.1289/EHP844).

The authors declare they have no actual or potential competing financial interests.

Received 20 July 2016; Revised 22 October 2016; Accepted 7 November 2016; Published 8 June 2017.

expression of CYP2B6 (Wei et al. 2012). In the present study, we assess the *in vivo* function of CYP2A13 and CYP2F1 in NA bioactivation and NA-induced respiratory tract toxicity in this novel mouse model. First, we developed a LC-MS/MS method for quantification of CYP2F1 protein in the TG mouse lung and nasal olfactory mucosa (OM), and compared CYP2F1 levels to the lung and OM expression levels of CYP2A13, which were previously determined by immunoblot analysis (Wei et al. 2012). For determination of metabolic activity of the transgenic CYP2A13 and CYP2F1, a CYP2A13/2F1-humanized version of the mouse model was utilized. This was necessary to avoid interference by mouse CYP2F2 and CYP2A enzymes, which are highly active in NA bioactivation (Hu et al. 2014; Li et al. 2011), and are expressed at much higher levels than the transgenic human CYPs in the mouse lung (Wei et al. 2012). The CYP2A13/2F1-humanized mouse was produced by intercrossing the TG mouse with a *Cyp2abfgs*-null mouse (Li et al. 2014), in which all mouse genes in the *Cyp2a, b, f, g, and s* gene subfamilies are deleted, yielding CYP2A13/2B6/2F1$^{(+)}$/*Cyp2abfgs*$^{(-/-)}$mice (designated as CYP2A13/2F1-humanized in this study, given that the transgenic CYP2B6 was not expressed in lung). To further distinguish the contributions of CYP2A13 from that of CYP2F1 to microsomal NA metabolism, a new CYP2A13-humanized mouse [CYP2A13$^{(+)}$/*Cyp2abfgs*$^{(-/-)}$] (Jia et al. 2014), with only CYP2A13 (but not CYP2B6 or CYP2F1) expressed, was also studied, to compare with the CYP2A13/2F1-humanized mice for *in vitro* metabolic activity toward NA, in conjunction with the use of an anti-CYP2A antibody. To determine the roles of CYP2A13/2F1 in NA-induced respiratory tract toxicity, the CYP2A13/2F1-humanized mice were compared to *Cyp2abfgs*-null mice for acute inhalation toxicity of NA *in vivo*. The extent of NA-induced lung and OM toxicity was assessed by histological analysis and through measurements of tissue levels of nonprotein sulfhydryl (NPSH), as well as biochemical markers for cytotoxicity.

Materials and Methods

Chemicals and Reagents

NA (99% pure, Lot# 0,732,804), glutathione (GSH), and NADPH were purchased from Sigma-Aldrich (St. Louis, MO). Acetaminophen-glutathione (AP-GSH) was purchased from Toronto Research Chemicals (Ontario, Canada). NA-GSH standard was a generous gift from Drs. Alan R. Buckpitt and Dexter Morin (University of California at Davis, Davis, CA). All solvents (acetonitrile, methanol, and water) were of high-performance liquid chromatography (HPLC) grade (Fisher Scientific, Houston, TX). Unless otherwise stated, all other chemicals and reagents were purchased from Sigma-Aldrich.

Animals

Homozygous CYP2A13/2B6/2F1-transgenic [2A13/2F1-TG$^{(+/+)}$] (Wei et al. 2012), *Cyp2abfgs*-null [*Cyp2abfgs*$^{(-/-)}$] (Li et al. 2014), and CYP2A13-humanized [2A13-TG$^{(+/-)}$ (i.e., hemizygous CYP2A13-only transgenic)/*Cyp2abfgs*$^{(-/-)}$] (Jia et al. 2014), as well as WT control, mice—all on C57BL/6 background—were obtained from breeding stocks maintained at the Wadsworth Center. 2A13/2F1-TG$^{(+/+)}$ mice were crossbred with *Cyp2abfgs*$^{(-/-)}$ mice, yielding 2A13/2F1-TG$^{(+/-)}$/*Cyp2abfgs*$^{(+/-)}$ mice, which, upon further crossbreeding with *Cyp2abfgs*$^{(-/-)}$ mice, produced 2A13/2F1-TG$^{(+/-)}$/*Cyp2abfgs*$^{(-/-)}$ mice. Given that only CYP2A13 and CYP2F1, but not CYP2B6, proteins are expressed in the respiratory tract (Wei et al. 2012), we named the 2A13/2F1-TG$^{(+/-)}$/*Cyp2abfgs*$^{(-/-)}$ mice "CYP2A13/2F1-humanized" mice for this study. All procedures involving animals were approved by the Institutional Animal Care and Use Committee of the Wadsworth Center. The animals were treated humanely with due consideration to the alleviation of distress and discomfort.

Methods for Detection and Quantification of CYP2F1 Protein

Tryptic probe peptide EALVDQGEEFSGR (>95% pure) for CYP2F1 was purchased from GenScript (Piscataway, NJ). The stable isotope-labeled probe peptide (internal standard) EALVDQGEEFSG[$R^{13}C^{15}N$] (>95% pure) was synthesized by Sigma-Aldrich (St. Louis, MO). RapiGest SF Powder was purchased from Waters (Milford, MA). Proteomics grade trypsin was purchased from Sigma-Aldrich. Sources of NA, NA-GSH, and AP-GSH were the same as described previously (Li et al. 2011).

The process of *in silico* selection of EALVDQGEEFSGR as the probe peptide for CYP2F1 detection and the method development for the LC-MS identification of the probe peptide are described in Supplemental Materials, "Methods Development for Detection of CYP2F1 Protein Using A Probe Peptide." The MS/MS spectra for EALVDQGEEFSGR and EALVDQGEEFSG[$R^{13}C^{15}N$] open are shown in Figure S1A.

Lung and OM microsomes from homozygous 2A13/2F1-TG$^{(+/+)}$ and WT mice were prepared according to a previously described protocol (Ding and Coon 1990). A recombinant CYP2F1 protein in insect Sf9 cell microsomes (Li et al. 2011) and normal Sf9 cell microsomes were used as positive and negative controls, respectively. A preparation of 100 µg microsomal protein was first denatured in 0.1% (W/V) RapiGest, a surfactant used to improve in-solution tryptic protein digestion (Yu et al. 2003). The denatured proteins were processed according to the following steps: *a*) reduction with DTT (added to a final concentration of 5 mM) and incubation at 60°C for 30 min; *b*) alkylation with iodoacetic acid (IAA, to a final concentration of 15 mM) and incubation in the dark, at room temperature, for 30 min; *c*) digestion with trypsin (proteomic grade) at an enzyme/substrate ratio of 1:100 by an overnight incubation at 37°C. Reactions were quenched by the addition of 5 M HCl (to a final concentration of 200 mM) and the mixtures were incubated at 37°C for 45 min, with shaking. Then the samples were centrifuged twice at 14,000 rpm in a model 5417C microcentrifuge from Eppendorf (Hauppauge, NY), at 4°C for 10 min each. The supernatant was collected, and desalted using Sep-Pak tC18 solid-phase extraction cartridges, prior to LC-MS/MS analysis.

The tryptic digests were analyzed by a LC-MS/MS system composed of an Agilent 1,200 Series HPLC and an ABI 4,000 Q-Trap mass spectrometer (Applied Biosystems, Foster City, CA), fitted with a XBridge BEH300 3.5-µm C18 column (150 × 2.1 mm, 300 A). The MS was operated in the positive ion mode, using electrospray ionization (ESI). The parameters for the chamber were source temperature, 450°C; curtain gas, 40 psi; declustering potential, 45 V; spray voltage, 4.6 kV; collision energy, 35 eV; and collision cell exit potential, 17 V.

The mobile phase consisted of solvent A [5% acetonitrile (ACN), 95% H_2O, 0.1% formic acid] and solvent B (95% ACN, 5% H_2O, 0.1% formic acid). The samples were eluted at a flow rate of 0.2 mL/min, with a linear increase from 0% B to 60% B between 2 and 15 min, followed by a wash at 60% B for 5 min. The mass spectrometer was operated in the multiple reaction monitoring (MRM) scan mode. Three most intensive MRM transitions for EALVDQGEEFSGR (*m/z* transitions 718.8/781.4, 718.8/1,024.4, 718.8/466.2) and their retention times were used for identification of CYP2F1 in the mouse microsomal samples.

The specificity of the optimized MRM transitions was confirmed by analyzing the tryptic digests of microsomal samples of *a*) Sf9 cells containing recombinant CYP2F1, *b*) control Sf9 cells, *c*) 2A13/2F1-TG$^{(+/+)}$ mice, and *d*) WT mice. Typical LC-MS chromatograms for the detection of EALVDQGEEFSGR in these tryptic samples are shown in Figure S1B.

The most intensive transition (*m/z* 718.8/781.4) of the probe peptide was used for quantitation of CYP2F1 in microsomal samples. The transition ion pair for the internal standard (EALVDQGEEFSG[$R^{13}C^{15}N$]) was 724.4/791.4. The retention times for EALVDQGEEFSGR and EALVDQGEEFSG[$R^{13}C^{15}N$] were both ~13.5 min. Authentic, purified probe peptide (0.05–20 pmol), as well as 1 pmol of internal standard, were spiked into 100 µg of control Sf9 cell microsomes and then processed as described above, for constructing calibration curves. The limit of detection (signal-to-noise ratio >3) for EALVDQGEEFSGR was 0.02 pmol on column, and the limit of quantification (signal-to-noise ratio >10) was 0.03 pmol on column. The recoveries of added standards in control Sf9 cell microsomes were >75%.

In Vitro *Assay of NA Bioactivation*

Incubations were performed in capped glass tubes as previously described (Li et al. 2011). Microsomes were prepared from pooled lung or OM tissues of male, 2-month-old *Cyp2abfgs*-null, CYP2A13-humanized, or CYP2A13/2F1-humanized mice. Reaction mixtures contained 50 mM phosphate buffer, pH 7.4, 1–200 µM NA (added in 1 µL methanol), 10 mM GSH, 0.20 mg/mL (for lung) or 0.05 mg/mL (for OM) microsomal protein, and 1 mM nicotinamide adenine dinucleotide phosphate (NADPH), in a final volume of 0.1 mL. The reaction was carried out at 37°C for 30 min for lung, or 15 min for OM, microsomal samples, and then quenched by the addition of two volumes of ice-cold methanol (containing 2 ng AP-GSH as internal standard). Rates were linear with incubation time under these conditions. The resultant mixtures were centrifuged to remove precipitated protein, and aliquots of the supernatant were used for NA-GSH determination by LC-MS/MS, as described previously (Li et al. 2011).

For immunoinhibition experiments, an anti-CYP2A5 antibody (Gu et al. 1998), which does not cross-react with CYP2F2 or CYP2F1 on immunoblots (data not shown), or a control IgG, was added to the reaction mixtures, to inhibit the lung and OM microsomal activity of *Cyp2abfgs*-null, CYP2A13-humanized, and CYP2A13/2F1-humanized mice. After all components for the *in vitro* assay (except NADPH and NA, but including control IgG and/or anti-CYP2A5 IgG, added at a combined level of 3 (for lung) or 4 (for OM) mg IgG/mg microsomal protein) were mixed in capped glass tubes, samples were preincubated on ice for 15 min, and then at 37°C for 3 min, followed by the addition of 100 µM NA and 1 mM NADPH to initiate the reaction at 37°C, as described above.

NA Inhalation Exposure

Two- to 3-month-old, *Cyp2abfgs*-null and CYP2A13/2F1-humanized mice (male, 3–6/group) were used in this experiment. Animals were exposed to NA vapor in a 24-port Oral-Nasal Aerosol Rodent Exposure System (CH Technologies, Westwood, NJ). The concentrations of NA vapor passing through the exposure system were achieved by adjusting the flow rates of fresh air and the air flowing through crystalline NA in a glass column heated to 52°C. Rates of air flow through each nose port were maintained at ~300 mL/min. Concentrations of NA in the chamber were determined in real time using a model IQ-604 Total Volatile Organic Compound Monitor containing a Photo-Ionization Detector sensor (Graywolf Sensing Solutions, Trumbull, CT), which was precalibrated by results of GC-MS analysis of NA concentration in gas samples collected from the inhalation chamber using precleaned (certified VOC-free) stainless steel 1-L canisters. Mice were exposed to NA vapor at 10 ppm, an OSHA (http://www.osha.gov/dts/chemicalsampling/data/CH_255800.html) permissible exposure limit for human workers, or to HEPA-filtered air (FA) as a control, for two 2-hr sessions, with a 30-min break in between (added to reduce stress to mice). The 4-hr total exposure time was selected to mimic daily occupational exposure. Immediately after exposure, blood samples were collected from the tail at various times (0 min to 2 hr) for preparation of plasma. Methods for determinations of plasma NA-GSH and NA were the same as previously described (Li et al. 2011). Two or 20 hr after termination of exposure, mice were euthanized and bronchoalveolar lavage (BAL) was conducted with Ca^{2+}- and Mg^{2+}-free phosphate-buffered saline (PBS), and the BAL fluid was used for cell counting and quantification of lactate dehydrogenase (LDH) activity and total protein levels, as previously described (Hubbs et al. 2001). These time points were selected according to previous studies in WT mice (Phimister et al. 2004). Tissue NPSH measurement and gross histopathological examination were performed as described previously (Li et al. 2011; Tonge et al. 1998). For liver and lung, one lobe was used for NPSH measurement, while a different lobe was used for histopathological examination; however, the same lobe was used for a given type of analysis. For nose, nasal cavity was fixed in Bouin's fixative and cut at levels 3, 5, and 6 (Young 1981) for histopathological examination. Another group of animals was used for NPSH measurement in OM.

High-Resolution Light Microscopy Examination of Airways and Quantitative Histopathology

Mice were exposed to NA vapor as described above. Twenty hours after termination of exposure, mice were euthanized and lungs were inflated and fixed with Karnovsky's fixative (0.9% glutaraldehyde/0.7% paraformaldehyde in cacodylate buffer, pH 7.4, 330 mOsmol/kgH_2O) as described previously (Van Winkle et al. 2001). Lungs were stored in the dark until use. Fixed left lobes were cut open to expose airways and embedded in Araldite 502 resin. Blocks were sectioned at 1 µm, and sections were stained with methylene blue azure II stain. Terminal bronchioles were imaged on an Olympus BH-2 microscope using Image Pro Plus image capture software. The volume fractions (V_v) were defined by point (P) and intercept (I) counting using a cycloid grid and Stereology Toolbox (Morphometrix, Davis, CA) for a minimum of 200 points. V_v was calculated using the formula $V_v = P_n/P_t$, where P_n is the number of test points hitting structures of interest (damaged epithelial cells), and P_t is the total points hitting the reference space (epithelial cells).

Other Methods

Protein concentration was determined by the bicinchoninic acid method (Pierce Chemical, Rockford, IL) with bovine serum albumin as the standard. Nonlinear regression and enzyme kinetic analyses were performed with use of GraphPad Prism 7 (GraphPad, San Diego, CA). One-way ANOVA (followed by Tukey's multiple comparisons test) was used to assess significance of differences among WT, CYP2A13-humanized and CYP2A13/2F1-humanized mice; between *Cyp2abfgs*-null and CYP2A13/2F1-humanized mice; or between FA exposure and NA exposure groups for each mouse strain.

Results

Expression Level of CYP2F1 Protein in Microsomal Samples of the Transgenic Mice

The relative CYP2F1 protein levels in the lung and OM microsomal preparations from WT and transgenic mice were previously estimated based on immunoblot analysis (Wei et al. 2012). A more precise quantitation of the actual levels was performed here using a newly developed LC-MS/MS method. The levels of CYP2F1 in a recombinant CYP2F1 preparation that was used previously as a standard for immunoblot quantitation (Wei et al. 2012), and those in lung and OM microsomes of 2A13/2F1-TG$^{(+/+)}$ mice, were found to be ~160, ~2, and ~8 pmol/mg protein, respectively. The 4-fold difference in CYP2F1 protein levels between lung and OM microsomes of the 2A13/2F1-TG$^{(+/+)}$ mouse agreed with previous immunoblot results (Wei et al. 2012). Compared to the levels of CYP2A13 protein in the lung (0.2 pmol/mg) and OM (100 pmol/mg protein) microsomes of the 2A13/2F1-TG$^{(+/+)}$ mouse (Wei et al. 2012), the levels of CYP2F1 were 10-fold higher in the lung, but 12-fold lower in the OM.

Role of CYP2A13 and CYP2F1 in NA Bioactivation in vitro

The activities of CYP2A13 and CYP2F1 toward NA were examined using microsomal samples from *Cyp2abfgs*-null, CYP2A13-humanized, and CYP2A13/2F1-humanized mice. The rates of NA-GSH formation were determined, with NA used at 1–200 μM. The apparent enzyme kinetic parameters are shown in Table 1 and the substrate-velocity curves are shown in Figure 1A. The apparent V_{max} values were higher, whereas the apparent K_M values were lower, in the lung and OM of the humanized mice, compared to *Cyp2abfgs*-null mice, resulting in higher catalytic efficiencies toward NA in CYP2A13-humanized mice (OM, ~4-fold; lung, ~2-fold) and CYP2A13/2F1-humanized mice (OM, ~6.5-fold; lung, ~9-fold). It is noteworthy that the apparent V_{max} values in the OM were substantially higher (~50-fold) than that in the lung, of the humanized mice, which was consistent with the much greater abundance of CYP2A13 in the OM than in the lung (Wei et al. 2012). Furthermore, the V_{max} values in the CYP2A13-humanized mice were significantly lower compared to those of CYP2A13/2F1-humanized mice, as was expected from the additional expression of CYP2F1 in the CYP2A13/2F1-humanized mice. However, given that CYP2A13 expression was somewhat higher (by ~35%) in CYP2A13/2F1-humanized mice than in CYP2A13-humanized mice (Jia et al. 2014), additional studies were conducted to distinguish between the contributions of CYP2F1 and CYP2A13, by selectively inhibiting the activity of CYP2A13.

An anti-CYP2A5 inhibitory antibody (Gu et al. 1998) was used to selectively inhibit CYP2A13 activity. The antibody cross-reacts with CYP2A13 (Wei et al. 2012), but it did not cross-react with recombinant CYP2F1 on immunoblots (data not shown). The rates of NA-GSH formation were determined in the presence of various amounts of anti-CYP2A5 IgG, while the total IgG levels were maintained constant by the addition of a control IgG. As shown in Figure 1B, with NA at 100 μM and at a level of 3 mg anti-CYP2A5 IgG/mg microsomal protein, the activities in the CYP2A13-humanized mice were nearly completely inhibited in OM and lung, reaching the background level observed in the *Cyp2abfgs*-null mice. The antibody also inhibited the activities in the CYP2A13/2F1-humanized mice; however, the residual activities at the saturating level of antibody added, which partly reflect contributions by CYP2F1, were still significantly higher than those of either CYP2A13-humanized or *Cyp2abfgs*-null mice. The additional activity in the CYP2A13/2F1-humanized mice relative to the CYP2A13-humanized mice is likely contributed by CYP2F1.

A comparison between lung and OM activity differences among the mouse strains in the absence or presence of anti-CYP2A5 also revealed tissue differences in the relative contributions by CYP2A13 and CYP2F1 (Figure 1B). It is evident that CYP2A13 played a much greater role in NA metabolism in the OM than in the lungs of the CYP2A13-humanized mice, and that CYP2F1 is not only active in NA bioactivation, but it played a significant role in NA metabolism in the lung of the CYP2A13/2F1-humanized mice.

Acute Inhalation Toxicity of NA in the CYP2A13/2F1-humanized Mouse

Inhalation studies were performed to evaluate the role of CYP2A13/2F1 in bioactivation of inhaled NA *in vivo* and in NA-induced toxicity in lung and OM. Plasma NA and NA-GSH levels were determined in *Cyp2abfgs*-null, CYP2A13/2F1-humanized, and WT mice after 4 hr of NA (10 ppm) inhalation. NA disposition was slower in both *Cyp2abfgs*-null and CYP2A13/2F1-humanized mice, compared to WT mice, as indicated by higher plasma NA levels and lower levels of the GSH-trapped metabolite NA-GSH (see Figure S2). There was no significant difference in plasma NA levels between *Cyp2abfgs*-null and CYP2A13/2F1-humanized mice, a result indicating that the respiratory tract-expressed CYP2A13/2F1 did not affect the systemic clearance of inhaled NA.

NA is known to induce respiratory tract toxicities, including observable lesions in the lung and OM, irrespective of the route of administration (Buckpitt et al. 2002). Mice were exposed to NA for 4 hr, a condition that mimics the occupational human exposure. To determine the role of CYP2A13/2F1 in NA toxicity *in vivo*, the extent of tissue toxicity was compared between the *Cyp2abfgs*-null and CYP2A13/2F1-humanized mice, with WT mice used as positive controls. Tissue NPSH levels and BAL fluid indices (LDH release, total protein recovery, and total cell counts), which are commonly used markers for cytotoxicity (Hubbs et al. 2001; Phimister et al. 2004), were measured at 2 and 20 hr after termination of NA inhalation (Figure 2). As

Table 1. Role of CYP2A13 and CYP2F1 in the formation of NA-GSH *in vitro* by lung and OM microsomes of humanized mice.[a]

	OM			Lung		
Strain	K_M (μM)	V_{max} (pmol/min/mg)	V_{max}/K_M (μL · mg^{-1} · min^{-1})	K_M (μM)	V_{max} (*pmol/min/mg*)	V_{max}/K_M (μL · mg^{-1} · min^{-1})
Cyp2abfgs-null	7.5 ± 2.6	124 ± 14	16.5	22.2 ± 4.9	8.8 ± 0.5	0.4
CYP2A13-humanized	10.6 ± 3.7	713 ± 82[b]	67.2	13.3 ± 0.6[c]	12.4 ± 0.3[b]	1.9
CYP2A13/2F1-humanized	10.2 ± 1.6	1070 ± 70[b,d]	105	7.1 ± 0.6[b]	24.5 ± 1.1[b,d]	3.5

[a]Apparent K_M and V_{max} values for the microsomal formation of NA-GSH were determined as described in "Materials and Methods" for CY2A13/2F1-humanized, CYP2A13-humanized, and *Cyp2abfgs*-null mice. Results represent means ± SD of values determined for three separate microsomal samples, each prepared from tissues pooled from five 2-month-old male mice.
[b]$p < 0.01$.
[c]$p < 0.05$, compared to corresponding tissues of *Cyp2abfgs*-null mice.
[d]$p < 0.01$, compared to corresponding tissues of CYP2A13-humanized mice (one-way ANOVA, followed by Tukey's multiple comparisons test).

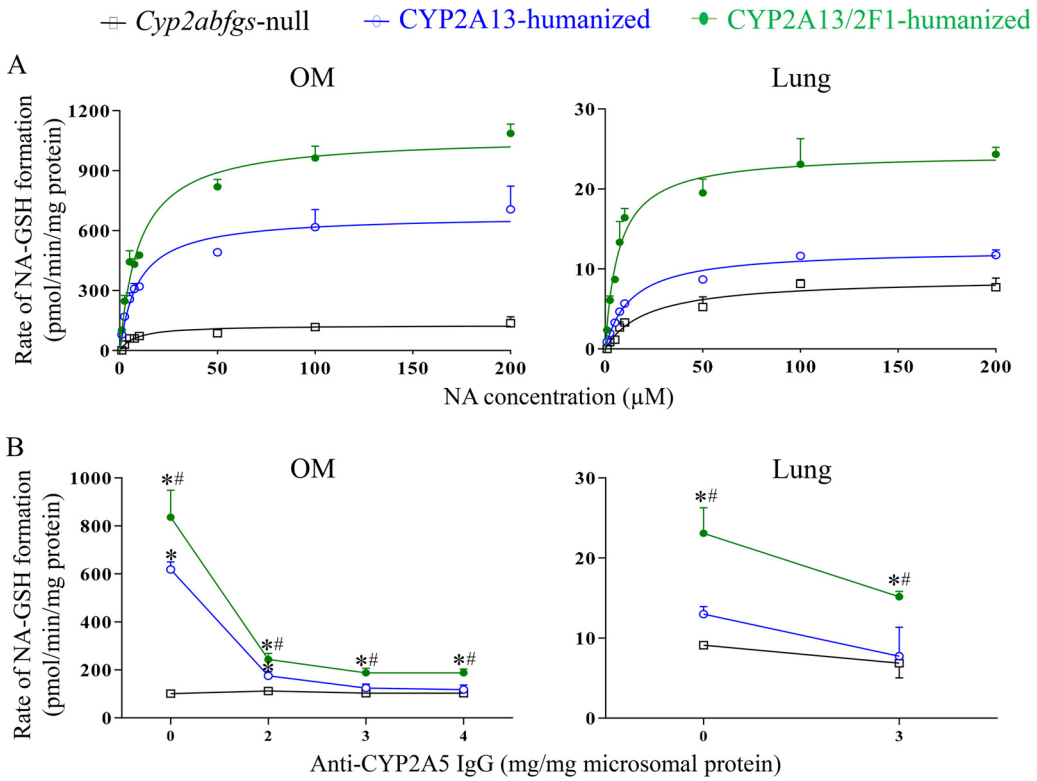

Figure 1. Metabolic activation of NA in CY2A13/2F1-humanized, CYP2A13-humanized, and *Cyp2abfgs*-null mice. Microsomes were prepared from three separate batches of pooled OM or lungs, each from five male, 2-months-old mice. (*A*) Substrate-velocity curves for *in vitro* NA-GSH formation by OM and lung microsomes. Contents of reaction mixtures are described in "Materials and Methods." The data (means ± SD, n = 3) were curve-fitted to the Michaelis-Menten equation. The calculated apparent kinetic parameters and results of statistical analysis are shown in Table 1. (*B*) Immunoinhibition of OM and lung NA metabolism by anti-CYP2A5 IgG. Contents of reaction mixtures are described in "Materials and Methods." Values represent means ± SD (n = 3). *, $p < 0.05$, compared to corresponding *Cyp2abfgs*-null mice; #, $p < 0.05$, compared to corresponding CYP2A13-humanized mice (one-way ANOVA, followed by Tukey's multiple comparisons test).

expected, the basal NPSH levels in lung and OM were similar among the different mouse strains when they were exposed to FA alone. Consistent with previous report on WT mice (Phimister et al. 2004), tissue NPSH levels were markedly lower than in NA-exposed than in FA-exposed WT mice, when measured at 2 hr after termination of NA inhalation, in both lung (by ~25%) and OM (by ~55%). Furthermore, the NA-induced NPSH depletion was not observed in either lung or OM of the *Cyp2abfgs*-null mice, a result confirming the role of mouse CYP2A/B/F/G/S enzymes in NA bioactivation in both lung and OM. However, NA-induced NPSH depletion was observed in OM (by ~45%), though not lung, of the CYP2A13/2F1-humanized mice. These data indicated that, at least in the OM, the transgenic CYP2A13/2F1 was able to bioactivate NA *in vivo* under the inhalation exposure condition used. When observed at 20 hr after termination of NA inhalation, no difference in lung NPSH levels was seen among the three mouse strains, exposed to either FA or NA, as the NPSH levels in the lung had already recovered to control levels in WT mice. However, NA-induced NPSH depletion persisted in the OM of CYP2A13/2F1-humanized mice, though only marginally so in WT mice, a result further supporting the role of CYP2A13/2F1 in bioactivating inhaled NA *in vivo*. Liver NPSH levels were also determined. As expected, there was no difference between strains or over postexposure time for the liver (data not shown), which is not a target for NA-induced toxicity. For BAL fluid cytotoxicity markers, WT mice, as expected, showed a remarkable increase in total cell counts, protein release, and LDH activity upon NA exposure, when measured at either time point, compared to mice exposed to FA (see Figure S3). However, these signs of NA-induced cytotoxicity were not observed in either the *Cyp2abfgs*-null or the CYP2A13/2F1-humanized mice, consistent with findings from NPSH measurements in the lungs of these mouse strains.

NA-induced Histopathologic Changes in the Lung and OM

Histopathologic examination was performed for lung and the olfactory regions of the nasal cavity (Figure 3). In all WT mice exposed to NA inhalation, airway epithelial cell necrosis was clearly visible in the lung using high-resolution light microscopy, at both time points after termination of exposure, with partial detachment of Club (Clara) cells from the bronchiolar epithelium. In contrast, NA-induced lung toxicity was not observed by routine light microscopy in paraffin sections in *Cyp2abfgs*-null or CYP2A13/2F1-humanized mice at either time point after termination of NA exposure. Consistent with previous findings with NPSH depletion, the *Cyp2abfgs*-null mice appeared to be fully protected from NA-induced nasal toxicity, whereas severe nasal toxicity was observed in both CYP2A13/2F1-humanized and WT mice following the NA inhalation exposure. Both CYP2A13/2F1-humanized and WT mice showed extensive injury to the OM, with evident epithelial necrosis, detachment, sloughing, and ulceration at either time points analyzed. No tissue toxicity was identified in any of the mouse strains exposed only to FA (data not shown).

High-resolution microscopic examination of airways, which is more sensitive and, when coupled with morphometry, quantitative than routine microscopy for measuring cytotoxicity, was performed to detect NA-induced lung toxicity at the cellular level. Normal and cytotoxic cells were defined based on their

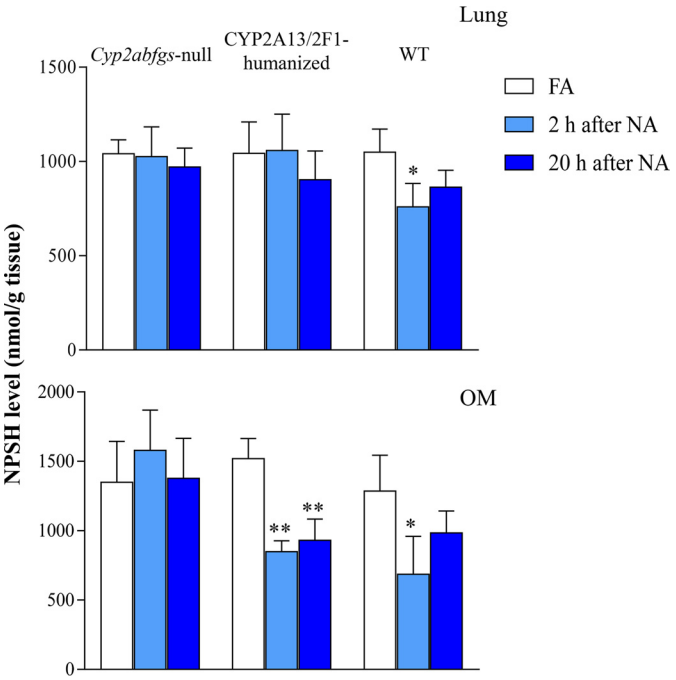

Figure 2. NPSH levels in lung and OM after exposure to FA or NA vapor. Two-month-old male *Cyp2abfgs*-null, CYP2A13/2F1-humanized, and WT mice were exposed to FA or NA vapor (10 ppm) for 4 hr. Tissues (lung and OM) were collected from individual mice for NPSH determination at 2 hr or 20 hr after termination of exposure. Data represent means ± SD (n = 3 ~ 6). *, $p < 0.05$, **, $p < 0.01$, compared to corresponding mice exposed to FA (basal level; at 2 or 20 hr, combined) for each strain (one-way ANOVA, followed by Tukey's multiple comparisons test).

morphologic appearance at high magnification on epoxy resin sections (Van Winkle et al. 1995). The cytotoxic cells were characterized by swelling, partial detachment from the basal lamina and/or vacuolization. (Figure 4). The volume fraction of cytotoxic (vs. total) terminal bronchiolar epithelial cells (V_v) was measured for all treatment groups (Table 2). Given no significant difference in V_v between FA-treated *Cyp2abfgs*-null group and FA-treated CYP2A13/2F1-humanized group, these two groups were pooled together as the FA-treated control group. Both NA-treated CYP2A13/2F1-humanized and NA-treated *Cyp2abfgs*-null groups had significantly greater volume fractions of cytotoxic epithelial cells than that in FA-treated control groups. Furthermore, greater epithelial cytotoxicity was observed in NA-treated CYP2A13/2F1-humanized mice (52.9% cells damaged) than in NA-treated *Cyp2abfgs*-null mice (<15% cells damaged) (Table 2). These results indicated that the expression of CYP2A13/2F1 in the humanized mouse resulted in increased sensitivity of the nasal and lung tissues to NA-induced cytotoxicity.

Discussion

CYP2F1 is predominantly expressed in the respiratory tract in humans (Carlson 2008; Weems and Yost 2010). There are significant species specific differences in CYP2F isoforms and their activity towards NA (Baldwin et al. 2004; Baldwin et al. 2005; Buckpitt et al. 2002). The expression of the human ortholog CYP2F1 in the lung has been implicated to be associated with tissue-specific toxicity induced by pulmonary toxicants, including NA, styrene, 3-methylindole, and benzene (Lanza et al. 1999; Nakajima et al. 1994; Powley and Carlson 2000). Conclusive data on the efficiency of CYP2F1 bioactivation in the *in vivo* microenvironment of the respiratory epithelium has not previously been demonstrated and thus the role of CYP2F1 bioactivation in chemical-induced toxicity was unknown.

In the present study, we provide definitive evidence that CYP2F1 is functional in NA bioactivation in lung microsomes, thus resolving a controversy in the field. We further demonstrate that, in CYP2A13/2F1-humanized mice, CYP2A13 and CYP2F1 are both active toward NA, and that the activity in the nasal mucosa and lung was primarily contributed by CYP2A13 and CYP2F1, respectively. Moreover, we show that transgenic expression of CYP2A13 and CYP2F1 in the *Cyp2abfgs*-null mice leads to exacerbation of nasal and lung toxicity induced by inhalation of NA at occupationally relevant exposure levels. These results ascertain the potential functional importance of both CYP2A13 and CYP2F1 in xenobiotic metabolism and toxicity in the respiratory tract. Our findings provide a solid foundation for further characterization of the expression and regulation of these tissue-specific CYP enzymes in the human respiratory tract, and their functions in the bioactivation and toxicity of numerous other xenobiotic compounds.

We have previously reported that the level of CYP2F1 protein expression in the lung and OM of the TG mice is much lower (by 10- to 40-fold) than the levels of its mouse ortholog CYP2F2 (Wei et al. 2012). Therefore, the TG mouse could not be used for direct analysis of the functions of the transgenic CYP2F1, given that the activities of CYP2F2 and other mouse P450s will mask the activities of the human CYP2F1. In order to abolish the activity of the endogenous mouse P450s, the TG mouse was cross-bred with a *Cyp2abfgs*-null mouse (Li et al. 2014). Our *in vitro* data show that the *Cyp2abfgs*-null mouse still had residual activities toward NA (Figure 1), implicating contributions by nonCYP2ABFGS enzymes. Nonetheless, the residual activities were far less efficient (Table 1), and thus were not high enough to mask activity of the transgenic human CYPs. It should also be noted that the catalytic efficiencies (V_{max}/K_M values) were much lower in lung microsomes from *Cyp2abfgs*-null mouse (0.4 μL/min/mg protein, Table 1, this study; K_M, 22.2 μM; V_{max}, 8.8 pmol/min/mg) compared to that in *Cyp2f2*-null mouse (2 μL/min/mg protein; K_M, 100 μM; V_{max}, 200 pmol/min/mg) (Li et al. 2011). This finding indicates contributions of CYP2A, 2B, and 2S enzymes, particularly the CYP2A enzymes (Hu et al. 2014), to NA metabolism in the mouse lung, and highlights the benefits of utilizing the *Cyp2abfgs*-null, instead of the *Cyp2f2*-null, mice for the production of CYP2A13/2F1-humanized mice.

CYP2A13 and CYP2F1 are co-expressed in the respiratory tract of humans and CYP2A13/2F1-humanized mice, and they are both active in NA bioactivation. In order to specifically identify the contributions of each enzyme to microsomal NA metabolism, we measured their relative expression levels in the lung and OM, compared the metabolic activity between CYP2A13/2F1-humanized and CYP2A13-humanized mice, and examined the effects of an anti-CYP2A antibody on microsomal NA bioactivation. In CYP2A13/2F1-humanized mice, CYP2F1 level is ~10-fold higher than CYP2A13 level in lung (2 vs. 0.2 pmol/mg protein), but it is ~10-fold lower than CYP2A13 level in the OM (8 vs. 100 pmol/mg protein). The CYP2A13/2F1-humanized mice had the highest V_{max} and catalytic efficiency (V_{max}/K_M) for microsomal NA bioactivation in both lung and OM, followed sequentially by CYP2A13-humanized mice and the background strain *Cyp2abfgs*-null mice (Table 1). The sequential decreases in V_{max} and catalytic efficiency in both lung and OM of these three mouse strains that differ only in their CYP2A13/2F1 genotypes indicate participation of both CYP2A13 and CYP2F1 in the microsomal activity in both organs. On the other hand, the relative extent of decreases in V_{max} from CYP2A13/2F1-humanized to CYP2A13-humanized mice (~33% for OM and ~49% for

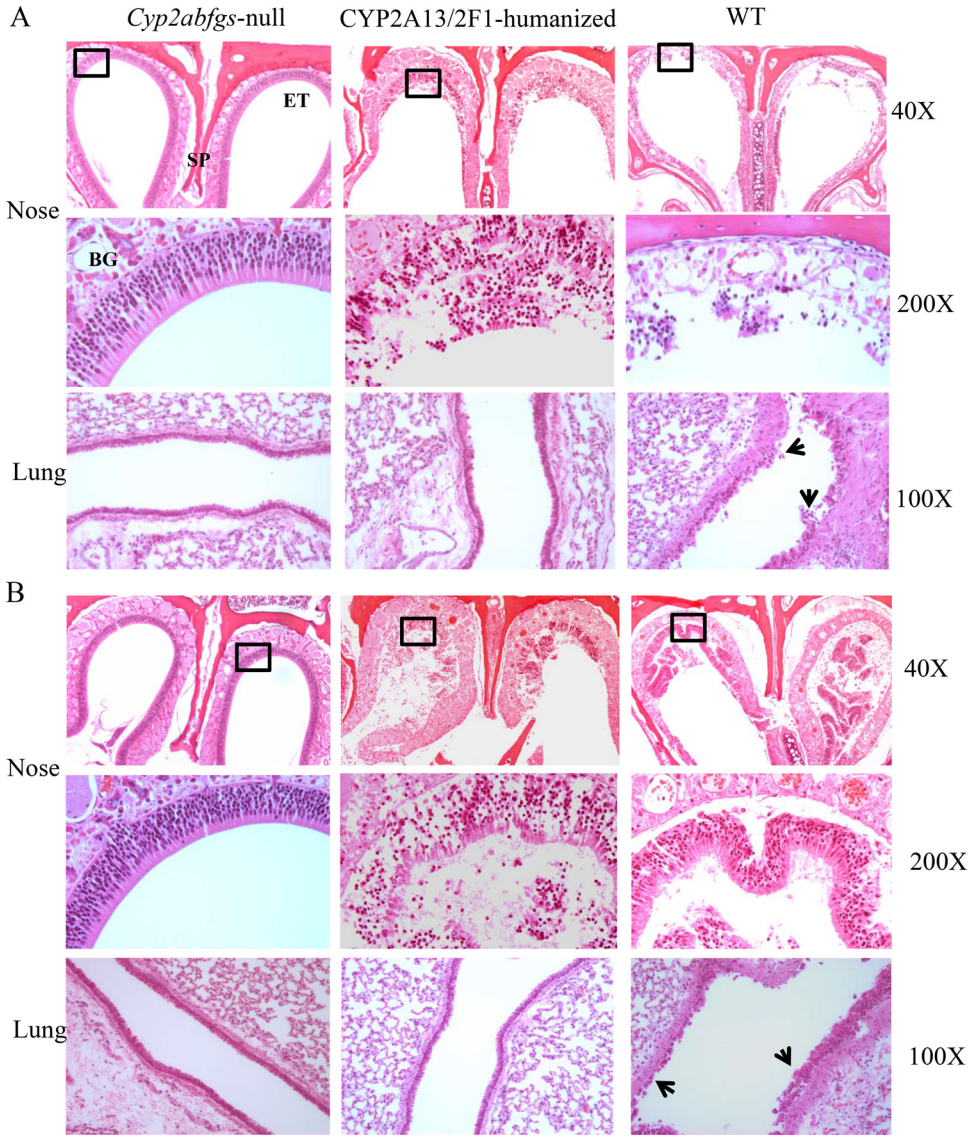

Figure 3. Histopathologic analysis of acute inhalation toxicity of NA in *Cyp2abfgs*-null, CYP2A13/2F1-humanized, and WT mice. Two- to 3-month-old male mice were exposed to FA or NA vapor (10 ppm) for 4 hr. Tissues (lung and nose) were obtained for histopathological examination at 2 hr (*A*) or 20 hr (*B*) after termination of NA inhalation. For the lung, representative hematoxylin and eosin-stained sections (100×) are shown. At either time point, NA-treated WT mice showed necrosis and detachment of Club cells and ciliated cells (arrow) from the epithelium; whereas NA-treated *Cyp2abfgs*-null and CYP2A13/2F1-humanized mice exhibited apparently normal epithelium. For the nose, hematoxylin and eosin-stained cross sections of the nasal cavity obtained at the level 3 of Young (Young 1981) are shown (at 40×); boxed areas, at the dorsal medial meatus, are shown below at 200×. At either time point, NA-treated WT and CYP2A13/2F1-humanized mice displayed signs of acute olfactory epithelial injury, including detachment of the mucosa, and the appearance of sloughed cells in the nasal cavity; whereas NA-treated *Cyp2abfgs*-null mice had normal ethmoidal turbinates (ET) lined by a thick, pseudostratified olfactory neuroepithelium, with Bowman's glands (BG) in the submucosa. SP, nasal septum. Data represent typical results from 3–6 mice in each group.

lung) and from CYP2A13-humanized to *Cyp2abfgs*-null mice (~83% for OM and ~29% for lung) indicates a greater role of CYP2A13 in the OM than in the lung and a greater role of CYP2F1 in the lung than in the OM. The CYP2A antibody-inhibition data (Figure 1B) further supports these conclusions, and allays any suspicion that the activity difference between the two humanized mouse models was due to contribution by CYP2B6. CYP2B6 has weak activity toward NA (Cho et al. 2006); however, although the CYP2A13/2F1-humanized mouse harbors a functional *CYP2B6* gene, CYP2B6 protein was not detected in the lung or OM of the TG mouse, with a detection limit of ~25 fmol/mg microsomal protein (Liu et al. 2015). It should also be noted that the apparent kinetic parameters determined for lung microsomes may underestimate activities in specific cell types, such as Club cells, which are known to contain higher levels of many P450 enzymes than parenchymal tissue (Baldwin et al. 2004; Lakritz et al. 1996) and may thus possess much greater catalytic efficiency (V_{max}/K_M) toward NA bioactivation.

The *in vitro* kinetic parameters for NA metabolism by CYP2A13/2F1-humanized mice were comparable to previously reported data from rhesus monkeys (Buckpitt et al. 2013). For example, monkey alveolar microsomes had a (V_{max}/K_M) of 17 μL/min/mg protein (K_M 1.14 μM, V_{max} 19 pmol/min/mg), compared to 3.5 μL/min/mg protein (K_M 7.1 μM, V_{max} 24.5 pmol/min/mg) for lung microsomes of CYP2A13/2F1-humanized mice. Monkey nasal epithelium had a V_{max} of 1,490 pmol/min/mg protein, compared to a V_{max} of 1,070 pmol/min/mg protein for OM of CYP2A13/2F1-humanized mice. The similarity between NA metabolic activity data for our humanized

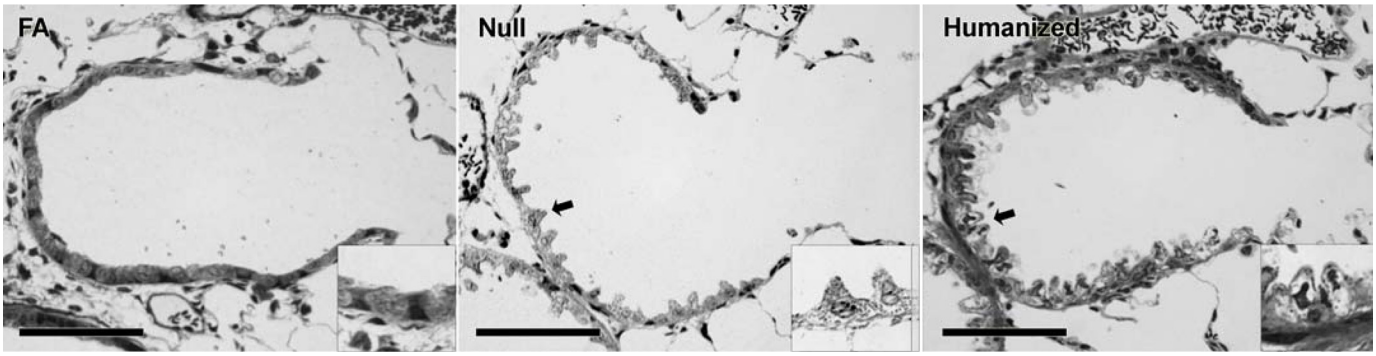

Figure 4. Representative high-resolution images of the epithelial damage in terminal bronchioles of mice exposed to FA or 10 ppm NA for 4 hr. Twenty hours after termination of exposure, mice were euthanized and lungs were inflated and fixed for histopathologic analysis as described in "Materials and Methods." In CYP2A13/2F1-humanized mice exposed to NA, evident epithelial cytotoxicity was observed, including cell swelling (arrow), partial detachment from the basal lamina, and/or vacuolization; the inset shows an enlarged view of swollen cells with darker nuclei staining, which signals cell death, and intracellular vacuoles. These signs of toxicity were also seen in FA-treated (FA) group or NA-treated *Cyp2abfgs*-null (Null) group, but less frequently, and to a lesser extent. Results of quantitative analysis of the extent of cellular injury in the various groups are shown in Table 2. Bar = 100 μm.

mouse and those of a nonhuman primate, the most reasonable surrogate for human metabolism of xenobiotics in the respiratory tract, highlights the value of our humanized mouse for studying the *in vivo* metabolism and toxicity of respiratory toxicants.

Our finding that both CYP2A13 and CYP2F1 are active toward NA in microsomes *in vitro* further supports the important role of CYP2A13/2F1 in NA-induced toxicity; the latter hypothesis was confirmed by the severe nasal toxicity caused by the 4 hr NA (10 ppm) inhalation exposure in the CYP2A13/2F1-humanized mice, compared to the absence of toxicity in the background strain *Cyp2abfgs*-null mice. However, the CYP2A13/2F1-mediated NA bioactivation in the lungs of the TG mice appeared to be insufficient to induce gross lung toxicity, a finding consistent with the relatively low expression of the human transgenes in that tissue. Nonetheless, the assays used for assessment of the gross lung toxicity, including routine histological analysis and measurements of lung levels of NPSH and biochemical markers for cytotoxicity, could not reveal cytotoxicity at the level of individual lung cells. Subsequent studies using high-resolution microscopy and morphometry revealed significantly greater NA-induced cellular damage in the terminal bronchioles of CYP2A13/2F1-humanized mice than in *Cyp2abfgs*-null mice, thus confirming the capability of CYP2A13/2F1-mediated NA bioactivation to cause cellular injury in both lung and nasal mucosa. The significance of the focal, rather than gross, lung toxicity should not be dismissed, given the focal nature of carcinogenesis, where tumors can arise from only a few transformed cells. In that connection, further studies to determine the regional distribution of CYP2A13/2F1 expression and activity toward NA in microdissected airways are warranted, in order to more precisely associate NA bioactivation with site-specific toxicity.

Table 2. Volume fraction (V_v) of cytotoxic bronchiolar epithelial cells in terminal bronchioles of mice exposed to NA or FA.[a]

Strain	Treatment	V_v of damaged cells (%)	Fold-Change (NA/FA)
Cyp2abfgs-null or CYP2A13/2F1-humanized[b]	FA	3.9 ± 1.7	
Cyp2abfgs-null	NA	14.6 ± 6.4[c]	3.7
CYP2A13/2F1-humamized	NA	52.9 ± 15.2[d,e]	13.6

[a]Two- to 3-month-old male mice were exposed to FA or NA vapor (10 ppm) for 4 hr. Lung samples were collected for fixation 20 hr after exposure, followed by high-resolution microscopic analysis, as described in "Materials and Methods." The abundance of cytotoxic bronchiolar epithelial cells was measured using morphometric procedures. The data represent means ± SD (n = 5). V_v was calculated as described in "Materials and Methods."
[b]There was no difference in the V_v of cytotoxic bronchiolar epithelial cells between FA-treated *Cyp2abfgs*-null and FA-treated CYP2A13/2F1-humanized group; therefore, these two groups were pooled together as the FA-treated control group.
[c]$p < 0.01$.
[d]$p < 0.001$, compared to FA-treated control group.
[e]$p < 0.001$, compared to NA-treated *Cyp2abfgs*-null group (one-way ANOVA, followed by Tukey's multiple comparisons test).

A physiologically based pharmacokinetic (PBPK) model for NA has been developed to support cross-species dosimetry comparisons of NA concentrations and tissue-normalized rate of metabolism (Campbell et al. 2014). This model estimates that NA concentrations in the lung following inhalation exposure are comparable between rodents and humans, which supports relevance of the *in vivo* data from rodent studies to human risk assessment. For example, with exposure at 10 ppm, NA concentration in the lung was estimated to be 0.87 nmol/g in rat and 0.84 nmol/g in human. Notably, the estimated tissue levels in the lung were much lower than those in the nose (25.6 nmol/g in rat OM and 88.6 nmol/g in human OM). Thus, if we assume that rats and mice have similar PBPK profiles, the estimated NA concentration in the lung of mice (~ 1 μM) is lower, while the estimated NA concentration in the OM (~ 25 μM) is higher, than the K_M for NA bioactivation (7–10 μM; Table 1), following 10-ppm NA inhalation. This dosimetry scenario is consistent with the greater toxicity seen in the OM than in the lung of the CYP2A13/2F1-humanized mice and, furthermore, it indicates that CYP2A13/2F1 is still capable of bioactivating NA to induce toxicity in airways at the estimated low tissue concentration of NA.

A novel LC-MS/MS method was developed in this study to quantify the absolute protein expression level of CYP2F1 in the TG mouse. Previous studies in the TG mouse detected CYP2F1 expression by immunoblot, but the absolute level of CYP2F1 protein was not determined; although heterologously expressed human CYP2F1 protein as used as a positive control, the absolute level of CYP2F1 in that positive control was unknown (Wei et al. 2012). LC-MS/MS-based methods for qualitative and quantitative determination of proteins in biological samples have the advantages of high specificity and sensitivity (Kamiie et al. 2008; Nagano et al. 2005; Seibert et al. 2009). The specificity of the optimized mass transitions for our *in silico*-selected CYP2F1 probe peptide was confirmed by analyzing the tryptic digests of Sf9 cell microsomal samples containing recombinant CYP2F1, and lung and OM microsomal samples from $TG^{(+/+)}$/$Cyp2f2^{(-/-)}$ mice, compared to microsomal samples from control Sf9 cells and $Cyp2f2^{(-/-)}$ mice, respectively. The sensitivity of CYP2F1 detection in our system was characterized by a

detection limit of ~0.3 pmol/mg microsomal protein. This level is comparable to reported detection limits for other membrane proteins using a similar type of mass spectrometer (Kamiie et al. 2008), is also close to the detection limit of immunoblot analysis for CYP2F1 (~0.1 pmol/mg protein; data not shown), and is substantially greater than the levels of CYP2F1 protein in the lung and OM of the TG mice (2 and 8 pmol/mg microsomal protein, respectively).

This new LC-MS/MS method will be useful for future studies that measure CYP2F1 protein expression levels in various biological samples, including human lungs. In that regard, though CYP2F1 mRNA expression was readily detected in human lung and OM (Hukkanen et al. 2002; Willey et al. 1996; Zhang et al. 2005), the levels of CYP2F1 protein in various microenvironments of the human respiratory tract have not been determined, partly due to the lack of a specific antibody to CYP2F1. Thus, further qualitative and quantitative analysis of CYP2F1 expression in human lung and OM will help to further assess the relevance of the findings in humanized mice to the potential toxicity of NA in humans.

Conclusion

Results of the present study indicate that CYP2A13 and CYP2F1 can both bioactivate NA *in vivo* and mediate nasal and lung toxicity induced by inhalation of NA at occupationally relevant exposure levels. The NA bioactivation activity in the nasal mucosa and lung was primarily contributed by CYP2A13 and CYP2F1, respectively.

Acknowledgments

We gratefully acknowledge the use of the services of the Pathology Core and the Advanced Light Microscopy and Image Analysis Core Facilities of the Wadsworth Center. We thank A. Buckpitt and D. Morin of UC Davis for providing NA-GSH standards; W. Yang for mouse breeding; and Q. Lin of the University at Albany Proteomics Core and Y. Weng of Pfizer Inc. for assistance with CYP2F1 quantitation using LC-MS/MS.

This work was supported in part by National Institutes of Health (NIH) grants CA092596, ES020867, and ES023513. The content is solely the responsibility of the authors and does not necessarily represent the official views of the NIH.

References

Abdo KM, Eustis SL, McDonald M, Jokinen MP, Adkins B, Haseman JK. 1992. Naphthalene: a respiratory tract toxicant and carcinogen for mice. Inhalation Toxicol 4:393–409, https://doi.org/10.3109/08958379209145317.

Abdo KM, Grumbein S, Chou BJ, Herbert R. 2001. Toxicity and carcinogenicity study in F344 rats following 2 years of whole-body exposure to naphthalene vapors. Inhal Toxicol 13:931–950, PMID: 11696867, https://doi.org/10.1080/089583701752378179.

Baldwin RM, Jewell WT, Fanucchi MV, Plopper CG, Buckpitt AR. 2004. Comparison of pulmonary/nasal CYP2F expression levels in rodents and rhesus macaque. J Pharmacol Exp Ther 309:127–136, PMID: 14724224, https://doi.org/10.1124/jpet.103.062901.

Baldwin RM, Shultz MA, Buckpitt AR. 2005. Bioactivation of the pulmonary toxicants naphthalene and 1-nitronaphthalene by rat CYP2F4. J Pharmacol Exp Ther 312:857–865, PMID: 15509722, https://doi.org/10.1124/jpet.104.075440.

Behrendorff JB, Moore CD, Kim KH, Kim DH, Smith CA, Johnston WA, et al. 2012. Directed evolution reveals requisite sequence elements in the functional expression of P450 2F1 in *Escherichia coli*. Chem Res Toxicol 25:1964–1974, PMID: 22901340, https://doi.org/10.1021/tx300281g.

Brusick D. 2008. Critical assessment of the genetic toxicity of naphthalene. Regul Toxicol Pharmacol 51:S37–S42, PMID: 17980943, https://doi.org/10.1016/j.yrtph.2007.08.013.

Buckpitt A, Boland B, Isbell M, Morin D, Shultz M, Baldwin R, et al. 2002. Naphthalene-induced respiratory tract toxicity: metabolic mechanisms of toxicity. Drug Metab Rev 34:791–820, PMID: 12487150, https://doi.org/10.1081/DMR-120015694.

Buckpitt A, Morin D, Murphy S, Edwards P, Van Winkle L. 2013. Kinetics of naphthalene metabolism in target and non-target tissues of rodents and in nasal and airway microsomes from the rhesus monkey. Toxicol Appl Pharmacol 270:97–105, PMID: 23602890, https://doi.org/10.1016/j.taap.2013.04.006.

Campbell JL, Andersen ME, Clewell HJ. 2014. A hybrid CFD-PBPK model for naphthalene in rat and human with IVIVE for nasal tissue metabolism and cross-species dosimetry. Inhal Toxicol 26:333–344, PMID: 24666369, https://doi.org/10.3109/08958378.2014.896059.

Carlson GP. 2008. Critical appraisal of the expression of cytochrome P450 enzymes in human lung and evaluation of the possibility that such expression provides evidence of potential styrene tumorigenicity in humans. Toxicology 254:1–10, PMID: 18951947, https://doi.org/10.1016/j.tox.2008.09.017.

Carr BA, Wan J, Hines RN, Yost GS. 2003. Characterization of the human lung *CYP2F1* gene and identification of a novel lung-specific binding motif. J Biol Chem 278:15473–15483, PMID: 12598524, https://doi.org/10.1074/jbc.M300319200.

Cho TM, Rose RL, Hodgson E. 2006. *In vitro* metabolism of naphthalene by human liver microsomal cytochrome P450 enzymes. Drug Metab Dispos 34:176–183, PMID: 16243959, https://doi.org/10.1124/dmd.105.005785.

Ding X, Coon MJ. 1990. Immunochemical characterization of multiple forms of cytochrome P-450 in rabbit nasal microsomes and evidence for tissue-specific expression of P-450s NMa and NMb. Mol Pharmacol 37:489–496, PMID: 2109181.

Fukami T, Katoh M, Yamazaki H, Yokoi T, Nakajima M. 2008. Human cytochrome P450 2A13 efficiently metabolizes chemicals in air pollutants: naphthalene, styrene, and toluene. Chem Res Toxicol 21:720–725, PMID: 18266326, https://doi.org/10.1021/tx700325f.

Gu J, Zhang QY, Genter MB, Lipinskas TW, Negishi M, Nebert DW, et al. 1998. Purification and characterization of heterologously expressed mouse CYP2A5 and CYP2G1: role in metabolic activation of acetaminophen and 2,6-dichlorobenzonitrile in mouse olfactory mucosal microsomes. J Pharmacol Exp Ther 285:1287–1295, PMID: 9618435.

Hu J, Sheng L, Li L, Zhou X, Xie F, D'Agostino J, et al. 2014. Essential role of the cytochrome P450 enzyme CYP2A5 in olfactory mucosal toxicity of naphthalene. Drug Metab Dispos 42:23–27, PMID: 24104196, https://doi.org/10.1124/dmd.113.054429.

Hubbs AF, Minhas NS, Jones W, Greskevitch M, Battelli LA, Porter DW, et al. 2001. Comparative pulmonary toxicity of 6 abrasive blasting agents. Toxicol Sci 61:135–143, PMID: 11294984.

Hukkanen J, Pelkonen O, Hakkola J, Raunio H. 2002. Expression and regulation of xenobiotic-metabolizing cytochrome P450 (CYP) enzymes in human lung. Crit Rev Toxicol 32:391–411, PMID: 12389869, https://doi.org/10.1080/20024091064273.

Jia K, Li L, Liu Z, Hartog M, Kluetzman K, Zhang QY, et al. 2014. Generation and characterization of a novel CYP2A13-transgenic mouse model. Drug Metab Dispos 42:1341–1348, PMID: 24907355, https://doi.org/10.1124/dmd.114.059188.

Kakareka SV, Kukharchyk TI. 2003. PAH emission from the open burning of agricultural debris. Sci Total Environ 308:257–261, https://doi.org/10.1016/S0048-9697(02)00650-2.

Kamiie J, Ohtsuki S, Iwase R, Ohmine K, Katsukura Y, Yanai K, et al. 2008. Quantitative atlas of membrane transporter proteins: development and application of a highly sensitive simultaneous LC/MS/MS method combined with novel *in-silico* peptide selection criteria. Pharm Res 25:1469–1483, PMID: 18219561, https://doi.org/10.1007/s11095-008-9532-4.

Lakritz J, Chang A, Weir A, Nishio S, Hyde D, Philpot R, et al. 1996. Cellular and metabolic basis of Clara cell tolerance to multiple doses of cytochrome P450-activated cytotoxicants. I: Bronchiolar epithelial reorganization and expression of cytochrome P450 monooxygenases in mice exposed to multiple doses of naphthalene. J Pharmacol Exp Ther 278:1408–1418, PMID: 8819528.

Lanza DL, Code E, Crespi CL, Gonzalez FJ, Yost GS. 1999. Specific dehydrogenation of 3-methylindole and epoxidation of naphthalene by recombinant human CYP2F1 expressed in lymphoblastoid cells. Drug Metab Dispos 27:798–803, PMID: 10383923.

Li L, Megaraj V, Wei Y, Ding X. 2014. Identification of cytochrome P450 enzymes critical for lung tumorigenesis by the tobacco-specific carcinogen 4-(methylnitrosamino)-1-(3-pyridyl)-1-butanone (NNK): insights from a novel *Cyp2abfgs*-null mouse. Carcinogenesis 35:2584–2591, PMID: 25173884, https://doi.org/10.1093/carcin/bgu182.

Li L, Wei Y, Van Winkle L, Zhang QY, Zhou X, Hu J, et al. 2011. Generation and characterization of a *Cyp2f2*-null mouse and studies on the role of CYP2F2 in naphthalene-induced toxicity in the lung and nasal olfactory mucosa. J Pharmacol Exp Ther 339:62–71, PMID: 21730012, https://doi.org/10.1124/jpet.111.184671.

Liu Z, Li L, Wu H, Hu J, Ma J, Zhang QY, et al. 2015. Characterization of CYP2B6 in a CYP2B6-humanized mouse model: inducibility in the liver by phenobarbital and dexamethasone and role in nicotine metabolism in vivo. Drug Metab Dispos 43:208–216, https://doi.org/10.1124/dmd.114.061812.

Nagano K, Taoka M, Yamauchi Y, Itagaki C, Shinkawa T, Nunomura K, et al. 2005. Large-scale identification of proteins expressed in mouse embryonic stem cells. Proteomics 5:1346–1361, PMID: 15742316, https://doi.org/10.1002/pmic.200400990.

Nakajima T, Elovaara E, Gonzalez FJ, Gelboin HV, Raunio H, Pelkonen O, et al. 1994. Styrene metabolism by cDNA-expressed human hepatic and pulmonary cytochromes P450. Chem Res Toxicol 7:891–896, PMID: 7696548.

Phimister AJ, Lee MG, Morin D, Buckpitt AR, Plopper CG. 2004. Glutathione depletion is a major determinant of inhaled naphthalene respiratory toxicity and naphthalene metabolism in mice. Toxicol Sci 82:268–278, https://doi.org/10.1093/toxsci/kfh258.

Powley MW, Carlson GP. 2000. Cytochromes P450 involved with benzene metabolism in hepatic and pulmonary microsomes. J Biochem Mol Toxicol 14:303–309, PMID: 11083083, https://doi.org/10.1002/1099-0461(2000)14:6<303::AID-JBT2>3.0.CO;2-8.

Seibert C, Davidson BR, Fuller BJ, Patterson LH, Griffiths WJ, Wang Y. 2009. Multiple-approaches to the identification and quantification of cytochromes P450 in human liver tissue by mass spectrometry. J Proteome Res 8:1672–1681, PMID: 19714871, https://doi.org/10.1021/pr800795r.

Shultz MA, Choudary PV, Buckpitt AR. 1999. Role of murine cytochrome P-450 2F2 in metabolic activation of naphthalene and metabolism of other xenobiotics. J Pharmacol Exp Ther 290:281–288, PMID: 10381788.

Su T, Bao Z, Zhang QY, Smith TJ, Hong JY, Ding X. 2000. Human cytochrome P450 CYP2A13: predominant expression in the respiratory tract and its high efficiency metabolic activation of a tobacco-specific carcinogen, 4-(methylnitrosamino)-1-(3-pyridyl)-1-butanone. Cancer Res 60:5074–5079, PMID: 11016631.

Tonge RP, Kelly EJ, Bruschi SA, Kalhorn T, Eaton DL, Nebert DW, et al. 1998. Role of CYP1A2 in the hepatotoxicity of acetaminophen: investigations using *Cyp1a2* null mice. Toxicol Appl Pharmacol 153:102–108, PMID: 9875304, https://doi.org/10.1006/taap.1998.8543.

U.S. EPA (U.S. Environmental Protection Agency). 1986. *Summary of Emissions Associated with Sources of Naphthalene.* EPA-450/3-88-003. Research Triangle Park, NC:U.S. EPA.

Van Winkle LS, Buckpitt AR, Nishio SJ, Isaac JM, Plopper CG. 1995. Cellular response in naphthalene-induced Clara cell injury and bronchiolar epithelial repair in mice. Am J Physiol 269:L800–L818, PMID: 8572242.

Van Winkle LS, Evans MJ, Brown CD, Willits NH, Pinkerton KE, Plopper CG. 2001. Prior exposure to aged and diluted sidestream cigarette smoke impairs bronchiolar injury and repair. Toxicol Sci 60:152–164, https://doi.org/10.1093/toxsci/60.1.152.

Weems JM, Yost GS. 2010. 3-Methylindole metabolites induce lung CYP1A1 and CYP2F1 enzymes by AhR and non-AhR mechanisms, respectively. Chem Res Toxicol 23:696–704, PMID: 20187624, https://doi.org/10.1021/tx9004506.

Wei Y, Wu H, Li L, Liu Z, Zhou X, Zhang QY, et al. 2012. Generation and characterization of a *CYP2A13/2B6/2F1*-transgenic mouse model. Drug Metab Dispos 40:1144–1150, PMID: 22397853, https://doi.org/10.1124/dmd.112.044826.

Willey JC, Coy E, Brolly C, Utell MJ, Frampton MW, Hammersley J, et al. 1996. Xenobiotic metabolism enzyme gene expression in human bronchial epithelial and alveolar macrophage cells. Am J Respir Cell Mol Biol 14:262–271, PMID: 8845177, https://doi.org/10.1165/ajrcmb.14.3.8845177.

Witschi H, Espiritu I, Maronpot RR, Pinkerton KE, Jones AD. 1997. The carcinogenic potential of the gas phase of environmental tobacco smoke. Carcinogenesis 18:2035–2042, PMID: 9395199.

Young JT. 1981. Histopathologic examination of the rat nasal cavity. Fundam Appl Toxicol 1:309–312, PMID: 6764423.

Yu YQ, Gilar M, Lee PJ, Bouvier ES, Gebler JC. 2003. Enzyme-friendly, mass spectrometry-compatible surfactant for in-solution enzymatic digestion of proteins. Anal Chem 75:6023–6028, PMID: 14588046, https://doi.org/10.1021/ac0346196.

Zhang QY, Ding X. 2008. The CYP2F, CYP2G and CYP2J subfamilies. In: *Cytochrome P450: Role in the Metabolism and Toxicity of Drugs and Other Xenobiotics*. Ioannides C, ed. Cambridge, UK:RSC Publishing, 309–353.

Zhang X, Zhang QY, Liu D, Su T, Weng Y, Ling G, et al. 2005. Expression of cytochrome P450 and other biotransformation genes in fetal and adult human nasal mucosa. Drug Metab Dispos 33:1423–1428, PMID: 16014766, https://doi.org/10.1124/dmd.105.005769.